УДК 620.9

Pioro I.[1]***, Zvorykina A.***[2]

[1] **University of Ontario Institute of Technology, Faculty of Energy Systems and Nuclear Science. Canada, Oshawa, Ontario**
[2] **National Technical University of Ukraine "Kiev Polytechnic Institute". Ukraine, Kiev**

SOME IMPORTANT ASPECTS FOR EXPERIMENTAL PAPERS: PART 2. UNCERTAINTY ANALYSIS

Анотація

В другій частині статті розглядається алгоритм аналізу похибок, який враховує основні принципи теорії термофізичних експериментів та їх похибок, базується на засадах сучасного досвіду проведення експериментів з теплопереносу і падіння тиску у воді, що знаходиться в надкритичному стані, а також на попередньому досвіді проведення експериментів з теплопереносу в умовах до критичного тиску.

Abstract

This Part 2 of the paper describes instrument calibrations and uncertainty calculations for the measured parameters such as temperature, pressure, pressure drop, mass-flow rate, power, geometrical dimensions, etc. and for the calculated parameters such as mass flux, heat flux, etc. in supercritical heat-transfer and pressure-drop tests.

1. General

The proposed uncertainty analysis[1] is based on our current experience with heat-transfer and pressure-drop experiments in supercritical water [1–2] and carbon dioxide [3] and on our long-term experience in conducting heat-transfer experiments at subcritical pressures [4–16]. Also, basic principles of the theory of thermophysical experiments and their uncertainties were applied [17–23].

In general, an uncertainty analysis is quite complicated process in which some uncertainties[2] (for example, uncertainties of thermophysical properties (for details, see NIST software [25]), uncertainties of constants, etc.) may not be known or may not be exactly calculated. Therefore, applying the engineering judgement is the only choice in some uncertainty calculations.

This section summarizes instrument calibrations and uncertainty calculations for the measured parameters such as temperature, pressure, pressure drop, mass-flow rate, power, tube dimensions, etc. and for the calculated parameters such as mass flux, heat flux, etc. in supercritical heat-transfer and pressure-drop tests. Uncertainties for these parameters are based on the RMS of component uncertainties. All uncertainty values are at the 2σ level, unless otherwise specified.

Calibration of the instruments used in the tests was performed either *in situ*, e.g., power measurements, test-section thermocouples, etc., or in an instrumentation shop, e.g., pressure transducers and bulk-fluid temperature thermocouples. In general, instruments were tested against a corresponding calibration standard.

When the same calibration standard is used for serial instruments, the calibration standard uncertainty is treated as a systematic uncertainty. In general, high accuracy calibrators were used, hence systematic errors for calibrated instruments are considered to be negligible. All other uncertainties are assumed to be random. Also, errors correspond to the normal distribution. Usually, the uncertainties have to be evaluated for three values of the corresponding parameter: minimum, mean and maximum value within the investigated range.

Uncertainties are presented below for instruments, which are commonly used in heat-transfer and pressure-drop experiments. It is important to know the exact schematics for sensor signal processing. Some commonly used cases, which are mainly based on a Data Acquisition System (DAS) recording, are shown in Figure 1 for thermocouples and in Figure 2 for Resistor Temperature Detectors (RTDs), pressure cells and differential-pressure cells.

Also, absolute and relative errors for commonly used functions are listed in Table 1 for reference purposes.

2. Temperature

For the calibrated thermocouples, the following linear characteristics were found:

$$V_{act} = a \cdot V_{meas} + b\,, \qquad (1)$$

[1] The authors of the current paper express their appreciation to D. Bullock and Y. Lachance (CRL AECL) for their help in preparation of this uncertainty analysis.

[2] Uncertainty refers to the accuracy of measurement standards and equals the sum of the errors that are at work to make the measured value different from the true value. The accuracy of an instrument is the closeness with which its reading approaches the true value of the variable being measured. Accuracy is commonly expressed as a percentage of a measurement span, measurement value or full-span value. Span is the difference between the full-scale and the zero scale value [24].

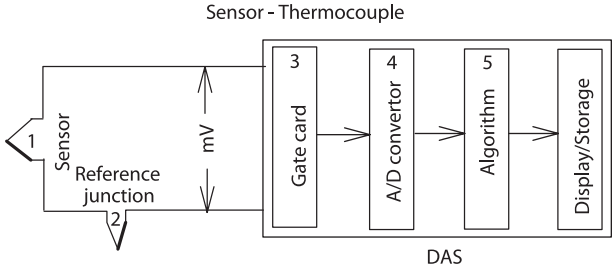

Figure 1. Schematic of signal processing for temperature (based on thermocouple) measurements. Numbers in figure identify uncertainty of particular device in measuring circuit: 1 — sensor uncertainty, 2 — reference junction uncertainty, 3 — Analog Input (A/I) uncertainty, 4 — Analog to Digital (A/D) conversion uncertainty, and 5 — DAS algorithm uncertainty

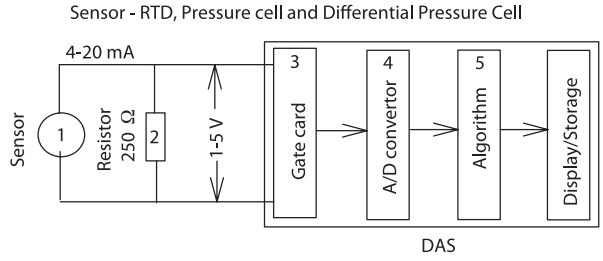

Figure 2. Schematic of signal processing for temperature (based on RTD), absolute pressure and differential pressure. Numbers in figure identify uncertainty of particular device in measuring circuit: 1 — sensor uncertainty, 2 — uncertainty due to temperature effect, 3 — A/I uncertainty, 4 — A/D conversion uncertainty, and 5 — DAS algorithm uncertainty; for RTD and both types pressure cells — DAS algorithm uncertainty is usually 0 due to linear fit

Table 1

Absolute and relative errors for commonly used functions (based on [22])

Function	Absolute error	Relative error
$Y = X_1 + X_2 + ... + X_n$	$\pm\sqrt{\Delta X_1^2 + \Delta X_2^2 + ... + \Delta X_n^2}$	$\pm\frac{\sqrt{\Delta X_1^2 + \Delta X_2^2 + ... + \Delta X_n^2}}{X_1 + X_2 + ... + X_n}$
$Y = \frac{X_1 + X_2 + ... + X_n}{n}$	$\pm\frac{\sqrt{\Delta X_1^2 + \Delta X_2^2 + ... + \Delta X_n^2}}{\sqrt{n}}$	$\pm\frac{\sqrt{n}\cdot\sqrt{\Delta X_1^2 + \Delta X_2^2 + ... + \Delta X_n^2}}{X_1 + X_2 + ... + X_n}$
$Y = X_1 - X_2$	$\pm\sqrt{\Delta X_1^2 + \Delta X_2^2}$	$\pm\frac{\sqrt{\Delta X_1^2 + \Delta X_2^2}}{X_1 - X_2}$
$Y = X_1 \cdot X_2$	$\pm\sqrt{(X_1\cdot\Delta X_2)^2 + (X_2\cdot\Delta X_1)^2}$	$\pm\sqrt{\left(\frac{\Delta X_1}{X_1}\right)^2 + \left(\frac{\Delta X_2}{X_2}\right)^2}$
$Y = a \cdot X$	$\pm a\cdot\Delta X$	$\pm\frac{\Delta X}{X}$
$Y = X^n$	$\pm n\cdot X^{n-1}\Delta X$	$\pm\frac{n\cdot\Delta X}{X}$
$Y = \sin X$	$\pm\cos X\cdot\Delta X$	$\pm\mathrm{ctg}X\cdot\Delta X$
$Y = \cos X$	$\pm\sin X\cdot\Delta X$	$\pm\mathrm{tg}X\cdot\Delta X$
$Y = \mathrm{tg}X$	$\pm\frac{\Delta X}{\cos^2 X}$	$\pm\frac{2\cdot\Delta X}{\sin(2\cdot X)}$
$Y = \mathrm{ctg}X$	$\pm\frac{\Delta X}{\sin^2 X}$	$\pm\frac{2\cdot\Delta X}{\sin(2\cdot X)}$

where V_{act} is the "actual" value [3] of the given parameter, V_{meas} is the value measured by the given instrument, and a and b are the calibration coefficients.

2.1 Measured Bulk-Fluid Temperature

The test section (see Figures 1 and 2 in Part 1 [29]) has three thermocouples to measure the inlet and outlet bulk-fluid temperatures. Also, the temperature at the flowmeter is monitored by thermocouple for fluid density calculations.

The test-section inlet and outlet bulk-fluid temperatures were measured with sheathed K-type thermocouples (for thermocouple signal processing, see Figure 1). These thermocouples were calibrated against the temperature standard RTD over the temperature range from 0 to 100 °C. For the reference RTD, the maximum error was ±0.3 °C. The maximum uncertainty of a data fit for inlet and outlet bulk-fluid temperature measurements is listed in Table 2.

The inlet and outlet bulk-fluid measurement uncertainties [4] are as follows:

Calibration system uncertainty	±0.3 °C
Thermocouple sensor accuracy after linear fit	±0.12 °C
A/I accuracy	±0.06 °C, i.e., ±0.025 % of f.s.; $\left(=\pm\frac{0.00025\cdot 10\ \text{mV}}{0.045\ \frac{\text{mV}}{\text{°C}}}\right)$; where f.s. is the full scale
A/D resolution accuracy (minimum 1 bit)	±0.03 °C $\left(=\pm\frac{10\ \text{mV (f.s.)}}{8192\ \text{counts}\cdot 0.045\ \frac{\text{mV}}{\text{°C}}}\right)$, where 0.045 mV/°C is the conversion rate, i.e., 4.509 mV for 100 °C [26]
Reference junction accuracy	±0.4 °C

For a given test-section inlet or outlet temperature t, the uncertainty Δt is given by

$$\frac{\Delta t}{t}=\sqrt{\left(\frac{0.3}{t}\right)^2+\left(\frac{0.12}{t}\right)^2+\left(\frac{0.03}{t}\right)^2}. \qquad (2)$$

The first term is the maximum error of the calibration system (±0.3 °C). The second term is the maximum error for the sheathed thermocouple (⩽100 °C), obtained from the calibration. The third term is the uncertainty introduced by the DAS, i.e., the A/D resolution uncertainty (±0.03 °C). Note that since the calibration was done *in situ* using the DAS as the measuring system for the RTD and for the calibrated thermocouples, the uncertainty introduced by the reference junction and the A/I accuracy was included in calibration curves.

Table 2

Linear coefficients for inlet and outlet temperature thermocouples (from instrument calibration records)

TC	Coefficient		Uncertainty, °C	Number of points
–	*a*	*b*	Maximum (2σ)	–
TE-1	1.000	–0.1798	0.12	5
TE-2	0.9980	0.1502	0.12	5
TE-3	0.9985	0.0980	0.12	5

All bulk-fluid temperature thermocouples were calibrated in situ, only within the range of 0–100 °C. Therefore, individual correction factors were implemented for each thermocouple within the range of 0–100 °C (see Table 2). For this range of temperatures, the uncertainty Δt is:

- for t_{min} = 20 °C Δt = ±0.32 °C (or ±1.62 %), and
- for t = 100 °C Δt = ±0.32 °C (or ±0.32 %).

Beyond this range, thermocouple uncertainties were taken as per [26], i.e., ±2.2 °C.

Thermocouple installed near the flowmeter was calibrated using another calibrating system and procedure. All inputs below are from instrument calibration record and device manuals unless otherwise specified.

Calibration system uncertainty:

±0.5°C, i.e., $\left(=\pm\sqrt{0.06^2+0.5^2+0.041^2}\right)$ where the first term is the accuracy of standard RTD, the second term is the accuracy of thermocouple signal measuring device and the third term is the accuracy of RTD signal measuring device (all uncertainties are in °C).

TC maximum calibration accuracy [5] (>2σ) within 0.0–45.0 °C	±0.53 °C
A/I accuracy	±0.06 °C, i.e., ±0.025 % of f.s. $\left(=\pm\frac{0.00025\cdot 10\ \text{mV}}{0.045\ \frac{\text{mV}}{\text{°C}}}\right)$

[3] The value obtained from the calibration standard.

[4] All inputs are from instrument calibration records and device manuals unless otherwise specified.

[5] The TC calibration accuracy is the maximum difference in °C between what the calibration standard measured and what TC indicated.

A/D resolution accuracy (minimum 1 bit)	$\pm 0.03\ ^\circ\text{C}\left(=\pm\dfrac{10\ \text{mV (f.s.)}}{8192\ \text{counts}\cdot 0.045\ \frac{\text{mV}}{^\circ\text{C}}}\right)$, where 0.045 mV/°C is the conversion rate, i.e., 4.509 mV for 100 °C [26]
Reference junction accuracy	±0.02 °C

For a given flowmeter bulk-fluid temperature t_{fm}, the uncertainty Δt_{fm} is given by

$$\left(\frac{\Delta t_{fm}}{t_{fm}}\right)_{TC}=\left(\pm\sqrt{\left(\frac{0.5}{t_{fm}}\right)^2+\left(\frac{0.53}{t_{fm}}\right)^2+\left(\frac{0.06}{t_{out}}\right)^2+\left(\frac{0.03}{t_{out}}\right)^2+\left(\frac{0.02}{t_{out}}\right)^2}\right)^2_{TC}. \quad (3)$$

Therefore, the flowmeter bulk-fluid temperature uncertainty is:

- for t_{fmmin} = 19 °C Δt_{fm} = ±0.74 °C (or ±3.9 %), and
- for t_{fmmax} = 35 °C Δt_{fm} = ±0.74 °C (or ±2.1 %).

Additional uncertainties due to thermocouple installation and possible electrical pickup have been minimized by using good engineering practices.

If a bulk-fluid temperature is measured with an RTD, then the following will apply.

The bulk-fluid temperature measurement uncertainties at the 2σ level are characterized with the following for an RTD (for RTD signal processing, see Figure 2).

Calibration system uncertainty in °C (from the instrument calibration record):

$$\text{Cal. Sys. Unc.}=\pm\sqrt{\left[\left(0.01\%\ \text{of Reading}\ \frac{16\ \text{mA}}{100^\circ\text{C}}+0.015\%\ \text{of f.s.}\right)\frac{100^\circ\text{C}}{16\ \text{mA}}\right]^2+(0.05^\circ\text{C})^2}\approx 0.06^\circ\text{C},$$

where the first term is the accuracy of calibrator in which reading is in °C and f.s. is 30 mA and a conversion rate is 16 mA for 100 °C; and the second term is the accuracy of standard RTD.

The RTD accuracy after linear fit, i.e., maximum deviation (from the instrument calibration record), is about ±0.08 °C;

A/I accuracy (from the device manual):
±0.032 °C (±0.025 % of f.s.), i.e.,

$$\left(=\pm\frac{0.00025\cdot 5.12\ \text{V (f.s.)}}{0.04\ \frac{\text{V}}{^\circ\text{C}}}\right).$$

A/D conversion accuracy (minimum 1 bit accuracy) (from the device manual):

$$\pm 0.016\ ^\circ\text{C, i.e.}\left(=\pm\frac{5.12\ \text{V (f.s.)}}{8192\ \text{counts}\cdot 0.04\ \frac{\text{V}}{^\circ\text{C}}}\right),$$

where 0.04 V/ °C is the conversion rate, i.e., 4 V for 100 °C (from the instrument calibration record).

DAS algorithm uncertainty is 0 due to a linear fit.

Therefore, for a given test-section inlet temperature, its uncertainty (Δt) is given by

$$\frac{\Delta t}{t}=\pm\sqrt{\left(\frac{\text{Cal. Sys. Unc.}}{t}\right)^2+\left(\frac{0.08}{t}\right)^2+\left(\frac{0.032}{t}\right)^2+\left(\frac{0.016}{t}\right)^2}. \quad (4)$$

The resulting uncertainties in the bulk-fluid temperature are

- For t = 10 °C Δt = ±0.10 °C (or ±1.2 %), and
- For t = 50 °C Δt = ±0.11 °C (or ±0.2 %).

If the bulk-fluid temperature is measured with several devices installed in a one cross section (for example, two RTDs and one thermocouple), the following equation may apply:

$$\frac{\Delta\bar{t}}{\bar{t}}\cong\pm\frac{\sqrt{(\Delta t_{RTD1})^2+(\Delta t_{RTD2})^2+(\Delta t_{TC})^2}}{\sqrt{3}\,\bar{t}}. \quad (5)$$

In this case, the resulting uncertainty will be close to the larger uncertainty, i.e., the thermocouple uncertainty. Therefore, if several devices have to be used for measuring a non-uniform temperature or any other parameter, they have to be with a similar accuracy.

2.2 External-Wall Temperature

Temperatures for the test-section external surface (see Figures 2 in Part 1 [29]) were measured using fast-response K-type thermocouples (see Figure 3). In general, thermocouple uncertainties for K-type thermocouples are ±2.2 °C within a range of 0–277 °C [26]. However, all fast-response thermocouples were calibrated *in situ* within a range of 0–100 °C prior to use (for details, see below). Therefore, individual correction factors were implemented for each thermocouple within the range of 0–100 °C. Beyond this range, thermocouple uncertainties were taken as per [26], i.e., ±2.2 °C.

All K-type thermocouples were calibrated against the temperature calibration standard (i.e., the reference RTD) over the temperature range from 0 to 100 °C. These thermocouple assemblies were immersed in a liquid bath thermostat together with the RTD. For the reference RTD, the maximum uncertainty is ±0.3 °C. The combined uncertainty[6] for wall temperature measurements is as follows:

[6] All inputs are from instrument calibration records and device manuals unless otherwise specified.

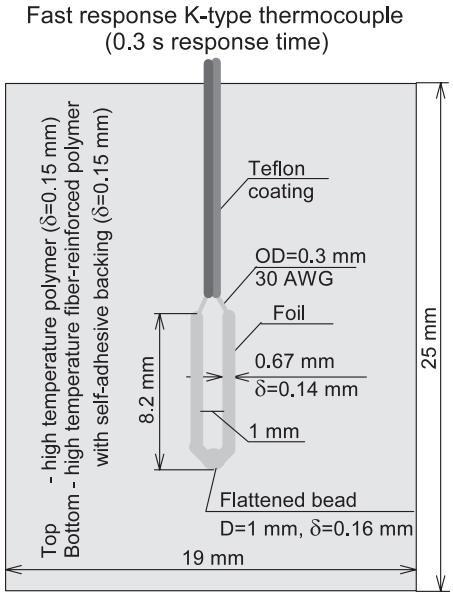

Figure 3. Sketch drawing of fast-response K-type thermocouple

Calibration system accuracy	±0.3 °C
Thermocouple sensor accuracy after linear fit	±0.16 °C max at values ⩽100 °C
A/I accuracy	±0.06 °C, i.e., ±0.025 % of f.s. $\left(=\pm\frac{0.00025\cdot 10\ \text{mV}}{0.045\ \frac{\text{mV}}{\text{°C}}}\right)$
A/D resolution accuracy (minimum 1 bit)	±0.03 °C $\left(=\pm\frac{10\ \text{mV (f.s.)}}{8192\ \text{counts}\cdot 0.045\ \frac{\text{mV}}{\text{°C}}}\right)$, where 0.045 mV/°C is the conversion rate, i.e., 4.509 mV for 100 °C [26]

For a given test-section wall temperature t, the uncertainty Δt is given by

$$\frac{\Delta t}{t}=\sqrt{\left(\frac{0.3}{t}\right)^2+\left(\frac{0.16}{t}\right)^2+\left(\frac{0.03}{t}\right)^2}. \qquad (6)$$

The first term is the maximum error of the calibration system (±0.3 °C). The second term is the maximum error of the sheathed thermocouple (⩽100 °C), obtained from the calibration. The third term is the uncertainty introduced by the DAS, i.e., the A/D resolution uncertainty (±0.03 °C). Note that since the calibration was done *in situ* using the DAS as the measuring system for the RTD and the calibrated thermocouples, the uncertainty introduced by the reference junction and the A/I accuracy was included in calibration curves.

Within the calibrated range of measured temperatures, i.e., from 0 to 100 °C, the uncertainty Δt is

- for t_{min} = 25 °C Δt = ±0.34 °C (or ±1.36 %), and
- for t = 100 °C Δt = ±0.34 °C (or ±0.34 %).

Also, the external wall temperatures measured with fast-response thermocouples were compared to the inlet and outlet bulk-fluid temperatures measured with sheathed thermocouples, at 0 power and 0 mass flux through the test section (see Figure 4). The comparison showed that, in general, all measured temperatures were within ±0.3 °C.

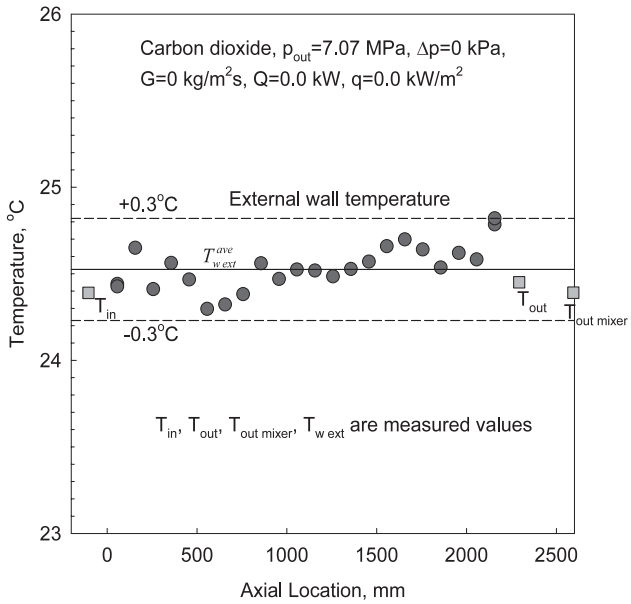

Figure 4. Temperature profile along test section at 0 power and 0 mass flux values

3. Absolute Pressure

A high-accuracy gauge pressure cell with a range of 0–10,000 kPa (0–10 MPa) was used for the outlet-pressure measurements (for pressure signal processing, see Figure 2). A small correction (77.2 kPa) is applied in the DAS program for the elevation difference between the pressure tap and transmitter. The combined uncertainty for absolute pressure measurements is as follows.

Accuracy of gauge pressure cell (from the calibration record) is ±0.1 % of calibrated span (10,000 kPa), and this accuracy was verified during the calibration check.

Calibration system uncertainty in kPa (from the instrument calibration record):

$$\text{Cal. Sys. Unc.}=\pm\sqrt{\left[\left(0.015\%\ \text{of Reading}\ \frac{16\ \text{mA}}{10000\ \text{kPa}}+0.015\%\ \text{of f.s.}\right)\frac{10000\ \text{kPa}}{16\ \text{mA}}\right]^2+(0\ .1\%\ \text{of Reading}\ )^2},$$

where the first term is the accuracy of calibrator in which reading is in kPa and f.s. is 30 mA and conversion rate is 16 mA for 10000 kPa; and the second term is the accuracy of tester.

Uncertainty due to temperature effect in 250-Ω resistor: ±0.1 %.

A/I accuracy (from the device manual): ±3.2 kPa, i.e., ±0.025 % of f.s., i.e., 5.12 V $\left(= \pm \frac{0.00025 \cdot 5.12\ \text{V}}{0.0004\ \frac{\text{V}}{\text{kPa}}} \right)$.

A/D conversion accuracy (minimum 1 bit accuracy) (from the device manual):

$$1.56\ \text{kPa}\ \left(= \pm \frac{5.12\ \text{V (f.s.)}}{8192\ \text{counts} \cdot 0.0004\ \frac{\text{V}}{\text{kPa}}} \right),$$

where 0.0004 V/kPa is the conversion rate, i.e., 4 V for 10,000 kPa (from the instrument calibration record).

For a given test-section outlet pressure p, the uncertainty Δp is given by

$$\frac{\Delta p}{p} = \pm \sqrt{\left(\frac{0.001 \cdot 10000}{p} \right)^2 + \left(\frac{0.1}{100} \right)^2 + \left(\frac{\text{A/I}}{p} \right)^2 + \left(\frac{\text{A/D}}{p} \right)^2}, \quad (7)$$

For the range of p from 7.6 to 8.8 MPa, the uncertainty Δp is given by

- for p_{min} = 7600 kPa Δp = ±13.1 kPa (or ±0.17 %),
- for p = 8400 kPa Δp = ±13.5 kPa (or ±0.16 %),
- for p_{max} = 8800 kPa Δp = ±13.8 kPa (or ±0.16 %).

4. Differential-Pressure Cells

Five differential-pressure transducers for measuring test-section pressure drops (for differential-pressure signal processing, see Figure 2) were connected to the corresponding pressure taps installed as shown in Figure 2, Part 1 [29]. They were used for measuring the test section axial pressure gradient and the overall pressure drop. Also, one differential-pressure transducer was used to measure a pressure drop across the flowmeter (see Figure 1, Part 1 [29]). All these pressure drops were measured using pressure transmitters.

A calibrator and a pressure module were used for the calibration check of the differential-pressure transducers. Basic characteristics of the test-section and flowmeter differential-pressure cells are listed in Table 3.

Accuracy, includes combined effects of linearity, hysteresis and repeatability in % of a calibrated span are listed in Table 3.

Calibration system uncertainty in kPa (from instrument calibration records):

$$\text{Cal. Sys. Unc.} = \pm \sqrt{\left[\left(0.015\%\ \text{of Reading}\ \frac{16\ \text{mA}}{\text{Span kPa}} + 0.015\%\ \text{of f.s.} \right) \frac{\text{Span kPa}}{16\ \text{mA}} \right]^2 + (0\ .05\%\ \text{of f.s.})^2},$$

where the first term is the accuracy of process calibrator in which reading is in kPa, f.s. is 30 mA and conversion rate is 16 mA for span in kPa; and the second term is the accuracy of calibrator in which f.s. is 690 kPa (100 psig (pounds per square inch, gage pressure).

Uncertainty due to temperature effect in 250-Ω resistor: ±0.1 %.

A/I accuracy (from a device manual):

$$\pm 0.025\ \%\ \text{of f.s., i.e.,}\ \left(= \pm \frac{0.00025 \cdot 5.12\ \text{V}}{\frac{4\ \text{V}}{\text{Span kPa}}} \right).$$

A/D conversion accuracy (minimum 1 bit accuracy) (from a device manual):

$$\left(= \pm \frac{5.12\ \text{V (f.s.)}}{8192\ \text{counts} \cdot \frac{4\ \text{V}}{\text{Span kPa}}} \right).$$

For a given pressure drop (Δp) for PDT-1, PDT-2 to PDT-5 and PDT-FM-1, the uncertainty $\Delta(\Delta p)$ is given by

$$\frac{\Delta(\Delta p)}{\Delta p} = \pm \sqrt{\left(\frac{\%\ \text{of span in kPa}}{\Delta p} \right)^2 + \left(\frac{0.1}{100} \right)^2 + \left(\frac{\text{A/I}}{\Delta p} \right)^2 + \left(\frac{\text{A/D}}{\Delta p} \right)^2}. \quad (8)$$

For the range of the total Δp from 5 to 70 kPa, the uncertainty $\Delta(\Delta p)$ for PDT-1 is given by

- for Δp_{min} = 5 kPa $\Delta(\Delta p)$ = ±1.50 kPa (or ±30.1 %), and
- for Δp_{max} = 70 kPa $\Delta(\Delta p)$ = ±1.51 kPa (or ±2.2 %).

For the range of the local Δp from 5 to 30 kPa, the uncertainty $\Delta(\Delta p)$ for PDT-2 — PDT-5 is given by

- for Δp_{min} = 5 kPa $\Delta(\Delta p)$ = ±0.25 kPa (or ±5.0 %), and
- for Δp_{max} = 70 kPa $\Delta(\Delta p)$ = ±0.25 kPa (or ±0.84 %).

For the local Δp equals to 37 kPa, the uncertainty $\Delta(\Delta p)$ for PDT-FM-1 is given by

- for Δp_{min} = 1.5 kPa $\Delta(\Delta p)$ = ±0.19 kPa (or ±12.5 %), and
- for Δp_{max} = 16.9 kPa $\Delta(\Delta p)$ = ±0.19 kPa (or ±1.1 %).

5. Mass-Flow Rate

The loop mass-flow rate FM-1 (see Figure 1, Part 1 [29]) is measured by a small orifice plate [7] with an orifice diameter of 0.308", and monitored by a differential-pressure

Table 3

Basic characteristics of differential-pressure cells

Instrument Name	Description	Output	Output kPa	Span kPa	Accuracy ±% of span
PDT-1	Total test-section pressure drop	10–50 mV	0–300	300	0.5
PDT-2	Test-section pressure drop	1–5 V	0–50	50	0.5
PDT-3	Test-section pressure drop	1–5 V	0–50	50	0.5
PDT-4	Test-section pressure drop	1–5 V	0–50	50	0.5
PDT-5	Test-section pressure drop	1–5 V	0–50	50	0.5
PDT-FM-1	Orifice-plate pressure drop	10–50 mV	0–37	37	0.5

cell with the range of 0–37 kPa. This cell has a square root output, with an accuracy of ±0.5 % of full scale.

The square root output is converted in the program to obtain kPa for use in the following flow equation, for a mass-flow rate of 0–0.24 kg/s (see Figure 5):

$$m = C_{fl} \sqrt{\rho \Delta p}\,, \qquad (9)$$

where $C_{fl} = 0.00130$ is the constant [27], ρ is the density at the orifice plate in kg/m^3, and Δp is the pressure drop across the orifice plate in kPa. It is known that orifice-plate flowmeters usually have a working range within (0.3 and 1)·m_{max}, i.e., 0.08–0.24 kg/s [28].

In general, the constant C_{flow} is a function of Reynolds number (see Figure 6). However, this effect is minor within the investigated range of Reynolds numbers (Re = 57,000–1,130,000).

We attempted to calibrate the flowmeter FM-1 with water using the direct weighting method [18] within the supercritical CO_2 investigated Reynolds numbers range. Due to significantly different values of water dynamic viscosity compared to those of supercritical carbon dioxide and restrictions applied to the maximum water flow and its temperature, the flowmeter was calibrated (see Figure 7) within a lower range of Reynolds numbers (Re = 2,700–27,000) compared to those of supercritical carbon dioxide (Re = 57,000–1,130,000).

However, the calibration results showed that Equation (9) is reasonably accurate (a mean error is −0.15% and an RMS error is 0.5%) for flows that are not less than 0.045 kg/s. This finding is consistent with heat-balance error data obtained in supercritical CO_2. However, the heat-balance error data for $m < 0.045$ kg/s

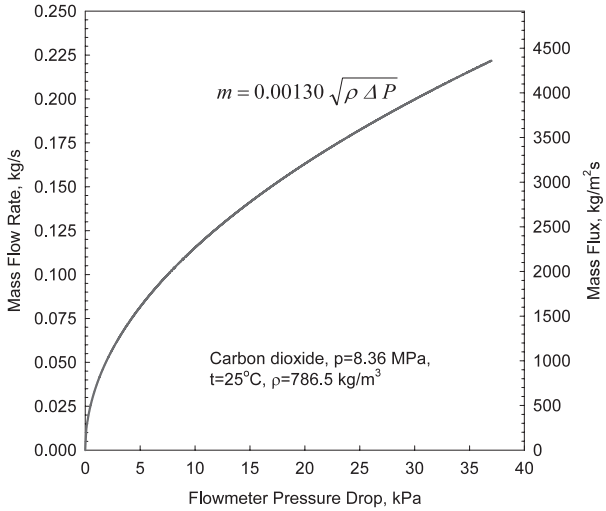

Figure 5. Flow-measurement curve

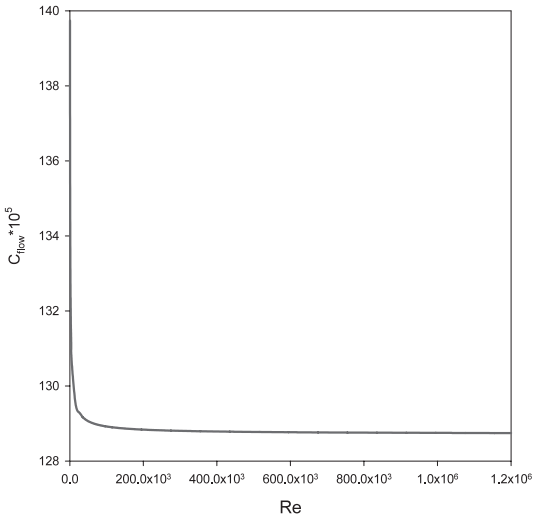

Figure 6. Effect of Reynolds number on flow constant

[7] This small diameter orifice plate is a non-standard orifice plate, because International Standard ISO 5167-2:2003(E), "Measurement of fluid flow by means of pressure differential devices inserted in circular-cross section conduits running full — Part 2: Orifice Plates", applies only to orifice plates with a diameter not less than 12.5 mm.

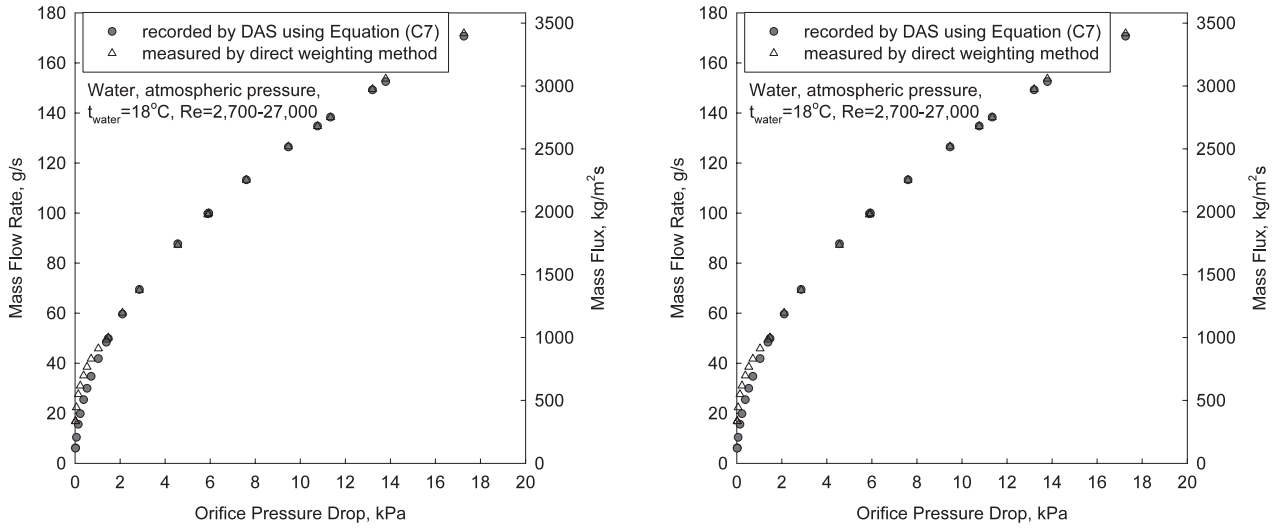

Figure 7. Calibration results for FM-1 orifice-plate flowmeter: (*a*) linear scale, and (*b*) logarithmic scale

show the opposite trend, i.e., steeper slope than that shown in Figure 7, *b*. Mass-flow rates lower than 0.045 kg/s were calculated using:

$$m = \frac{POW}{H_{out} - H_{in}}. \qquad (10)$$

In general, flow-rate measurement uncertainty within the range of $m = 0.045–0.24$ kg/s is given by:

$$\frac{\Delta m}{m} = \sqrt{\left(\frac{\Delta C_1}{C_1}\right)^2 + \left(\frac{0.5\,\Delta\rho}{\rho}\right)^2 + \left(\frac{0.5\,\Delta(\Delta p)}{\Delta p}\right)^2}. \qquad (11)$$

The estimated uncertainty in the constant C_1 is ±0.08 % as a result of the minor effect of Reynolds number on the constant within the investigated range [27].

Temperature, pressure (see Figure 1, Part 1 [29]) and NIST software (2010) [25] were used for the CO_2 density calculation. At pressures up to 30 MPa and temperatures up to 249.9 °C (523 K), the estimated uncertainty in density [25] varies up to 0.05 %. Also, additional uncertainty in density arises from variations in density within the measured temperature uncertainty of ±1.1 °C. This additional uncertainty is about ±1.1 % at $p = 8.36$ MPa and $t = 19$ °C, and ±5.0% at $p = 8.8$ MPa and $t = 35$ °C. Therefore, the total uncertainty in density is

$$\frac{\Delta\rho}{\rho} = \sqrt{\left(\frac{0.05}{100}\right)^2 + \left(\frac{1.1}{100}\right)^2} = 0.011 \qquad (12)$$

at $p = 8.36$ MPa and $t = 19$ °C

and

$$\frac{\Delta\rho}{\rho} = \sqrt{\left(\frac{0.05}{100}\right)^2 + \left(\frac{5.0}{100}\right)^2} = 0.05 \qquad (13)$$

at $p = 8.8$ MPa and $t = 35$ °C.

However, the vast majority of the experimental data were obtained at pressure of 8.36 MPa. Therefore, the uncertainty value of 0.011 was used below.

Pressure-drop measurement uncertainties for PDT-FT-1/1 are according to Section 4.

Hence,

- for $m_{min} = 46$ g/s $\Delta m = \pm 5.7$ g/s (or ±12.5 %) at $t = 19$ °C and $p = 8.36$ MPa,

and

- for $m_{max} = 155$ g/s $\Delta m = \pm 2.4$ g/s (or ±1.6 %) at $t = 19$ °C and $p = 8.36$ MPa.

6. Mass Flux

Mass flux, G, is based on mass-flow rate measurements. The uncertainty, ΔG, includes an error in the estimation of the cross-sectional flow area, $A_{fl} = 5.1 \cdot 10^{-5}$ m^2. The test section is a tube of 8.058 mm ID and 10 mm OD, made of Inconel 600, with tolerances of ±0.02 mm. The uncertainties are as follows:

For ID $\Delta D = \pm 0.02$ mm (or ±0.25 %),

For OD $\Delta D_{ext} = \pm 0.02$ mm (or ±0.20 %),

and

For A_{flow} $\Delta A_{fl} = \frac{\pi D \Delta D}{2} = \pm 0.253$ mm^2 (or ±0.50%).

The uncertainty, ΔG, is obtained from the following equation:

$$\frac{\Delta G}{G} = \sqrt{\left(\frac{\Delta m}{A_{fl} G}\right)^2 + \left(\frac{m\,\Delta A_{fl}}{A_{fl}^2 G}\right)^2} = \sqrt{\left(\frac{\Delta m}{m}\right)^2 + \left(\frac{\Delta A_{fl}}{A_{fl}}\right)^2}. \qquad (14)$$

For the range of interest, the uncertainties, ΔG, are:

- for $G_{min} = 902$ kg/m^2·s ($m_{min} = 46$ g/s) $\Delta G = \pm 112.8$ kg/m^2·s (or ±12.5 %), and
- for $G_{max} = 3039$ kg/m^2·s ($m_{max} = 155$ g/s) $\Delta G = \pm 49.8$ kg/m^2·s (or ±1.6 %).

7. Electrical Resistivity

Electrical resistivity is a calculated value that is based on measured values of electrical resistance, heated length and tube diameters.

The accuracy of the micro-ohmmeter used in test-section electrical resistance measurements is ±0.04 % of the reading (its readings are in milliohms). The uncertainties in ID and OD are $\Delta D = D_{ext} = \pm 0.02$ mm, and in L it is $\Delta L = \pm 0.5$ mm.

For a given electrical resistivity, the uncertainty $\Delta\rho$ is given by

$$\frac{\Delta\rho_{el}}{\rho_{el}} = \sqrt{\left(\frac{0.04}{100}\right)^2 + \left(\frac{\Delta D_{ext}}{D_{ext}}\right)^2 + \left(\frac{\Delta D}{D}\right)^2 + \left(\frac{\Delta L}{L}\right)^2}. \quad (15)$$

The uncertainty in $\Delta\rho_{el}$ ($\rho_{el} = 104.3\cdot10^{-8}$ Ohm·m) is

• for $L = 2461$ mm $\Delta\rho_{el} = \pm 0.212\cdot10^{-8}$ Ohm·m (or ±0.20 %).

8. Total Test-Section Power

The total test-section power is obtained by measuring the current through a 2000 A/100 mV current shunt and the voltage across the test section. These signals are fed into a Power-Measuring Unit (PMU), where the test-section voltage is scaled down to a 1-V level. Both the voltage and current signals are fed into isolation amplifiers and then into instrumentation amplifiers with outputs of 0–10 V. The amplifier outputs are fed to the computer analog inputs and represent a full-scale voltage of 175 V and a full-scale current of 2000 A. These signals are multiplied in the computer program to represent a 0–350 kW power level.

Calibration of the power measurement unit was performed *in situ*. Test-section voltage and current inputs were removed from the PMU. Simulated inputs were used to check the calibration of the unit. A comparison between the computer readings and the calibrated simulated inputs was used to create a curve fit for the DAS to correct for the differences. The voltage input from 0–110 V DC was simulated with a DC power supply and verified with a multimeter. The current shunt input was simulated with a calibrator for inputs from 10 to 100 mV, which represents 200 – 2000-A range:

Accuracy of current shunt	±0.25 % of reading
Error due to current shunt resistance change	±0.02 %
A/D accuracy	0.025 % of f.s., 10.00 V

The uncertainty, ΔPOW_{TS}, in power measurements (the power is a product of U and I) is given by

$$\frac{\Delta POW_{TS}}{POW_{TS}} = \sqrt{\left(\frac{0.25}{100}\right)^2 + \left(\frac{0.02}{100}\right)^2 + \left(\frac{0.1}{100}\right)^2 + \left(\frac{0.09}{100}\right)^2 + \left(\frac{\Delta I_1}{I}\right)^2 + \left(\frac{\Delta U_1}{U}\right)}. \quad (16)$$

The first term is the accuracy of the current shunt, the second term is the effect of a temperature change on the current shunt, the third term is the error in the test-section voltage drop from the PMU output of $\Delta U = +0.1$ % (0.10 V) up to 100 V, the fourth term is the error in the test-section current from the PMU output with a maximum offset of $\Delta I = +0.09$ % (0.75 A) at 800 A, and the fifth and sixth terms are the ±0.025 % uncertainties introduced by the AC/DC conversion process for reading the current ($\Delta I_1 = \pm 0.5$ A) and ($\Delta U_1 = \pm 0.04$ V) for reading the voltage, respectively.

For the power range, POW_{TS}, from 3.0 to 35.0 kW, and for $L = 2.208$ m, the corresponding values of voltage drop and current are

• $POW_{TS\,min} = 3000$ W $U = 16.0$ V, $I = 188$ A, and
• $POW_{TS\,max} = 35{,}000$ W $U = 54.6$ V, $I = 641$ A.

The uncertainty in ΔPOW_{TS} is as follows:

• For $POW_{TS\,min} = 3000$ W
$\Delta POW_{TS} = \pm 13.9$ W (or ±0.46 %), and
• For $POW_{TS\,max} = 35{,}000$ W
$POW_{TS} = \pm 106.4$ W (or ±0.30 %).

9. Average Heat Flux

The uncertainty in heat flux, Δq_{ave}, involves the uncertainties in the total test-section power (see Section 8) and in the heated area measurements, ΔA_h, where $A_h = \pi DL$. The uncertainty in ID is $\Delta D = \pm 0.02$ mm, and in L it is $\Delta L = \pm 0.5$ mm. Thus, ΔA_h can be calculated from

$$\frac{\Delta A_h}{A_h} = \sqrt{\left(\frac{\Delta D}{D}\right)^2 + \left(\frac{\Delta L}{L}\right)^2}. \quad (17)$$

The uncertainty in A_h ($A_h = 55{,}895.4$ mm^2) is

• For $L = 2208$ mm and $D = 8.058$ mm
$\Delta A_h = \pm 78.3$ mm^2 (or ±0.14 %).

Then, the uncertainty in q_{ave} can be computed from

$$\frac{\Delta q_{ave}}{q_{ave}} = \sqrt{\left(\frac{\Delta POW_{TS}}{POW_{TS}}\right)^2 + \left(\frac{\Delta A_h}{A_h}\right)^2}, \quad (18)$$

which, for the given power values, results in

• $q_{ave\,min} = 53.7$ kW ($POW_{TS} = 3.0$ kW)
$\Delta q = \pm 0.28$ kW/m^2 (or ±0.53 %), and
• $q_{ave\,max} = 626.2$ kW ($POW_{TS} = 35.0$ kW)
$\Delta q = \pm 2.46$ kW/m^2 (or ±0.39 %).

However, Equation (18) does not account for the uncertainties related to the heat loss, which are subtracted from the applied heat flux, because the heat loss was negligible, i.e., less than 0.5 %.

10. Uncertainties in Heat Transfer Coefficient

Local HTC is as follows:

$$HTC = \frac{q}{t_w^{\text{int}} - t_b}. \qquad (19)$$

Uncertainty in the temperature difference is

$$\frac{\Delta(t_w^{\text{int}} - t_b)}{t_w^{\text{int}} - t_b} = \pm \frac{\sqrt{\left(\Delta t_w^{\text{int}}\right)^2 + \left(\Delta t_b\right)^2}}{t_w^{\text{int}} - t_b}, \qquad (20)$$

where uncertainty in t_w^{int} is taken as uncertainty in t_w^{ext} and uncertainty in t_b is taken as uncertainty in t_{out}. And uncertainty ΔHTC is:

$$\frac{\Delta HTC}{HTC} = \sqrt{\left(\frac{\Delta q}{q}\right)^2 + \left(\frac{\Delta(t_w^{\text{int}} - t_b)}{t_w^{\text{int}} - t_b}\right)^2}. \qquad (21)$$

11. Uncertainties in Thermophysical Properties near Pseudocritical Point

Uncertainties in thermophysical properties [25] near the pseudocritical point within the uncertainty range of the measured value of bulk-fluid temperature ($\Delta t = \pm 0.4$ °C) are as follows (for example, at $p = 8.38$ MPa ($t_{pc} = 36.7$ °C)):

$\Delta\rho = \pm 7$ %; $\Delta H = \pm 2.5$ %; $\Delta c_p = 4.5$ %; $\Delta k = \pm 2$ %, and $\Delta\mu = \pm 7$ %.

12. Heat-Loss Tests

Heat loss is an important component of the total heat-balance analysis. Heat loss from the test section, HL_{TS}, to the surrounding area was measured at various wall temperatures, with electrical power applied to the test section (the loop was previously evacuated to minimise heat removal through the coolant). This test provided (*i*) an indication of the difference between the measured external wall temperatures and ambient temperature, and (*ii*) data (voltage and current applied to the test section) to calculate the heat loss from the test section.

To perform the heat loss power test, a small power supply was used.

The temperature difference between the external wall temperatures and ambient temperature at zero power was found to be ±0.2 °C (i.e., within the accuracy range for the thermocouples); with an increase in power to the test section, the difference ($\Delta t = t_w^{ave} - t_{amb}$) increases. This temperature difference permits the evaluation of the heat loss from the test section to the surrounding area as follows:

$$HL_{TS} = POW_{TS} = f(\Delta t), \qquad (22)$$

or, as calculated,

$$HL_{TS} = POW_{TS} = U I, \qquad (23)$$

where U is the voltage drop over the test section, and I is the current through the test-section wall. This heat loss test, compared to the usual zero-power test, eliminates uncertainties that are related to the estimation of the thermophysical properties of CO_2. This test also eliminates flow-measurement uncertainties and uncertainties that are incurred when measuring very small temperature differences (0.5–1 °C) between the inlet and outlet bulk-fluid temperatures.

The heat-loss power test was performed with the insulated reference test section (heated length of 2.208 m). The heat loss assessed from these tests, as a function of the wall-ambient temperature difference, ($t_w^{ave} - t_{amb}$), is shown in Figure 8, and can be approximated by the following equation:

$$HL_{TS} = 0.47\left(t_w^{ave} - t_{amb}\right) \text{[W]}. \qquad (24)$$

There were some non-uniformities in the temperature distribution along the heated length. These non-uniformities were caused by the power clamps and structural support elements for the test section, which acted as heat sinks. Therefore, a conservative approach (maximum possible heat loss and therefore, minimum HTC value) was taken, i.e., only two external wall thermocouples (TECO01 and TECO24), which are located in the same cross-sections as TECO02 and TECO23, respectively, but 180° apart, were not taken into account (see Figure 2, Part 1 [29]).

For local heated lengths, the following formula would apply:

$$HL_{TS}\Big|_{L\ell} = HL_{TS}\Big|_{L=2.208m} \frac{L_\ell}{2.208} \text{ [kW]}, \qquad (25)$$

where $L\ell$ is in metres.

In general, heat loss was negligible, i.e., less than 0.5 %.

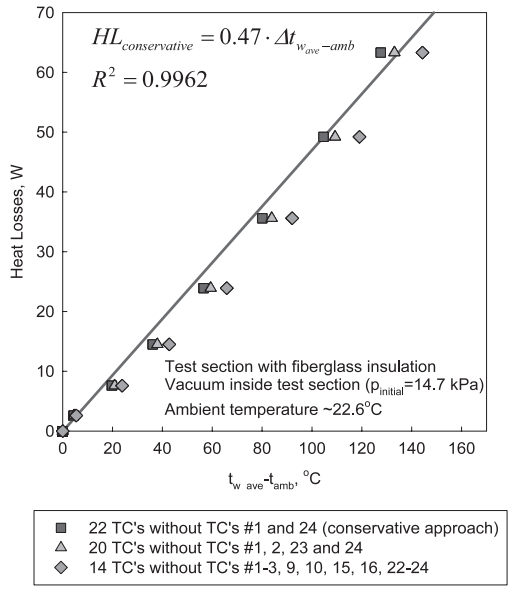

Figure 8. Heat loss from test section: Direct electrical heating of test section, heated length of 2.208 m, and loop vacuumed

13. Heat-Balance Evaluation near Pseudocritical Region

For each run, an error in the heat balance was calculated using the following expression:

$$\Delta_{HB} = \frac{POW - HL - m\,(H_{out} - H_{in})}{POW} \cdot 100\% \,. \quad (26)$$

In general, an analysis of errors in the heat-balance data shows that, at mass-flux values equal to or higher than 900 kg/m^{2}s, at medium and high values of power ($POW \geqslant 5$ kW) and at the inlet and outlet bulk-fluid temperatures below or beyond the pseudocritical region (i.e., t_{in} and $t_{out} < t_{pc} - 2$ °C or t_{in} and $t_{out} > t_{pc} + 2$ °C), these errors are within ±4 %.

Increased values of heat-balance error (i.e., more than ±4 %) at lower values of power ($POW < 5$ kW) and at inlet or outlet bulk-fluid temperatures within the pseudocritical region (i.e., $t_{pc} - 2$ °C $< t_{in} < t_{pc} + 2$ °C or $t_{pc} - 2$ °C $< t_{out} < t_{pc} + 2$ °C) can be explained with the following (see Table 4 and Figure 9).

At lower values of power, the increase in bulk-fluid enthalpy is relatively small. However, uncertainties in bulk-fluid enthalpy within the pseudocritical region are larger for the same uncertainty range in bulk-fluid temperature, compared to the enthalpy values' uncertainties that correspond to temperatures far from the pseudocritical region.

Also, an additional error in the heat balance appears at mass-flux values below 900 kg/m^{2}s (see Figure 7), where the flow-measuring curve is steep. Therefore, lower values of mass flux should be measured with a smaller diameter orifice flowmeter[8] or other type flowmeters.

Figure 9 shows an example of the heat-balance evaluation near the pseudocritical region. This graph shows that, at lower power values ($POW < 5$ kW) and at the outlet bulk-fluid temperature within the pseudocritical region, variations in bulk-fluid enthalpy difference can be up to 11.5 % within the nominal uncertainty range for bulk-fluid temperatures (i.e., ±0.4 °C).

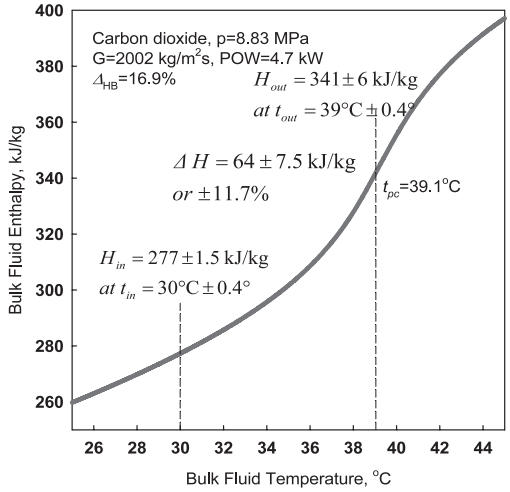

Figure 9. Heat-balance evaluation near pseudocritical region

Conclusions

Part 1 [29] of this paper presents a detailed description of a typical heat-transfer / thermlahydraulics test facility for supercritical carbon dioxide and provides practical recommendations for performing experiments. And Part 2 of this paper describes instrument calibrations and uncertainty calculations for the measured parameters such as temperature, pressure, pressure drop, mass-flow rate, power, geometrical dimensions, etc. and for the calculated parameters such as mass flux, heat flux, etc. in supercritical heat-transfer and pressure-drop tests. This experimental paper is based on requirements from the nuclear industry for performing tests and, therefore, can be used as a sample for high-quality experimental studies in various areas.

Table 4

Maximum uncertainties in ΔH calculations near pseudocritical point (p_{out} = 8.36 MPa, t_{pc} = 36.7 °C, t_{in} = 21 °C, m = 0.1 kg/s, and G = 2000 kg/m^{2}s)

t_b	H_b	Uncertainty in H_b at Δt_b = +0.4 °C	Uncertainty in H_b at Δt_b = –0.4 °C	$\Delta H_b = H_{out} - H_{in}$	Max uncertainty in ΔH_b
°C	kJ/kg	kJ/kg	kJ/kg	kJ/kg	%
21	248.94	1.18	–1.19	–	–
35	313.72	4.29	–5.04	64.78	14.4
37	349.26	8.51	–7.82	100.32	16.3
41	395.75	2.56	–2.4	144.41	3.4

[8] However, orifice-plate flowmeters with a diameter of the orifice less than 12.5 mm is considered a non-standard type.

Symbols and abbreviations

A area, m^2
A_{fl} flow area, m^2
c_p specific heat at constant pressure, J/kg K
$\bar{c}_p$ averaged specific heat within the range of $(T_w - T_b)$; $\left(\frac{H_w - H_b}{T_w - T_b}\right)$, J/kg K
D inside diameter, m
D_{ext} external diameter, m
D_{hy} hydraulic diameter, m; $\left(\frac{4\,A_{fl}}{P_{wetted}}\right)$
f friction factor; $\left(\frac{\sigma_w}{\frac{G^2}{8\,\rho}}\right)$
f_d drag coefficient
G mass flux, kg/m^2s; $\left(\frac{m}{A_{fl}}\right)$
g gravitational acceleration, m/s^2
H specific enthalpy, J/kg
h heat transfer coefficient, W/m^2K
HL heat loss, W
I current, A
K_{ir} neutron-flux irregularity coefficient
k thermal conductivity, W/m K
L heated length, m
L_{tot} total length, m
m mass-flow rate, kg/s; (ρV)
P, p pressure, MPa
POW power, W
Q power or heat-transfer rate, W
q heat flux, W/m^2;
q_v volumetric heat flux, W/m^3; $\left(\frac{Q}{V_h}\right)$
R molar gas constant, 8.31451 J/mol K
R radius, m
R_a arithmetic average surface roughness, μm
R_{bend} radius of bending (for tube)
R_{el} electrical resistance, Ohm
r radial coordinate or radius, m; regression coefficient
s specific entropy, J/kg K
T, t temperature, °C
U voltage, V
u axial velocity, m/s
V volume, m^3 or volumetric flow rate, m^3/s
V_m molar volume, m^3/mol
v specific voume, m^3/kg;
v radial velocity, m/s
x axial coordinate, m
x steam content
y radial distance; $(r_0 - r)$, m
z axial coordinate, m

Greek Letters

α thermal diffusivity, m^2/s; $\left(\frac{k}{c_p\,\rho}\right)$
β volumetric thermal expansion coefficient, 1/K
Δ difference
Δ_{HB} error in heat balance, %
δ thickness, mm
ε dissipation of turbulent energy
μ dynamic viscosity, Pa s
π reduced pressure; $\left(\frac{p}{p_{cr}}\right)$
π steam-reheat-loop power to evaporating-looppower ratio
P perimeter, m
ρ density, kg/m^3
ρ_{el} electrical resistivity, Ohm·m
σ dispersion
σ_w viscous stress, N/m^2
υ kinematic viscosity, m^2/s
ξ friction coefficient

Non-dimensional Numbers

Ga Galileo number; $\left(\frac{g\,D^3}{\nu^2}\right)$
Gr Grashof number; $\left(\frac{g\,\beta\,\Delta T\,D^3}{\nu^2}\right)$
Gr_q modified Grashof number; $\left(\frac{g\,\beta\,q_w\,D^4}{k\,\nu^2}\right)$
Nu Nusselt number; $\left(\frac{h\,D}{k}\right)$
Pr Prandtl number; $\left(\frac{\mu\,c_p}{k}\right)=\left(\frac{\upsilon}{\alpha}\right)$
$\bar{Pr}$ averagedPrandtl number within the range of $(t_w - t_b)$; $\left(\frac{\mu\ \bar{c}_p}{k}\right)$
Re Reynolds number; $\left(\frac{G\,D}{\mu}\right)$
Ra Raleigh number; (GrPr)

St	Stanton number; $\left(\frac{Nu}{Re\,Pr}\right)$

Symbols with an overbar at the top denote average or mean values (e.g., Nu denotes average (mean) Nusselt number).

Subscripts or superscripts

ac	acceleration
amb	ambient
ave	average
b	bulk
cal	calculated
cr	critical
cr sect	cross section
dht	deteriorated heat transfer
el	electrical
ext	external
f	fluid
fl	flow
fm	flowmeter
fr	friction
g	gravitational
h	heated
HB	Heat Balance
hor	horizontal
hy	hydraulic
in	inlet
int	internal
iso	isothermal
ℓ	liquid or local
m	molar
main	refers to main or primary steam directed toturbine
max	maximum
meas	measured
min	minimum
nom	nominal or normal
0	constant properties, scale, reference, characteristic, initial, or axial value
out	outlet or outside
OD	outside diameter
pc	pseudocritical
r	reduced
reheat	refers to secondary or reheat steam directed to turbine
T	value of turbulent flow
TS	test section
th	thermal or threshold value
tot	total
v	volumetric (vapour)
vert	vertical
w	wall
wt	weight

Abbreviations and acronyms widely used in the text and list of references

ABWR	Advanced Boiling Water Reactor
AC	Alternating Current
ACR	Advanced CANDU Reactor
A/D	Analog-to-Digital (conversion)
A/I	Analog Input
AECL	Atomic Energy of Canada Limited (Canada)
AERE	Atomic Energy Research Establishment (UK)
AGR	Advanced Gas-cooled Reactor
AIAA	American Institute of Aeronautics and Astronautics
AIChE	American Institute of Chemical Engineers
ANS	American Nuclear Society
AP	Advanced Plant or Acidification Potential
aq	aqueous
ASME	American Society of Mechanical Engineers
ASHRAE	American Society of Heating, Refrigerating and Air-conditioning Engineers
AWG	American Wire Gauge
BBL (bbl)	barrels of oil (unit)
BWR	Boiling Water Reactor
CANDU	CANada Deuterium Uranium nuclear reactor
CCE	Ceramic Carbon Electrodes
CCS	Carbon Capture and Sequestration (or Storage)
CEA	Commissariat à l'Énergie Atomique (French Atomic Energy Commission)
CFD	Computational Fluid Dynamics
CFP	Carbon Fiber Paper
CHF	Critical Heat Flux
CRL	Chalk River Laboratories, AECL (Canada)
CV	Cyclic Voltammetry
DALY	Disability-Adjusted Life Years
DAS	Data Acquisition System
DC	Direct Current
DOE	Department Of Energy (USA)
DP	Differential Pressure
emf	electromotive force
EGP	Power reactor Graphite-moderated with Steam overheat (in Russian abbreviations)
ENS	European Nuclear Society
EP	Eutrophication Potential
EPR	European Pressurized Reactor
EU	European Union
EXT	EXTernal

FA	Fuel Assembly
FBR	Fast Breeder Reactor
FC	Fluoro-Carbon
FM	FlowMeter
F/M	Ferritic-Martensitic (steel)
FR	Fuel Rod
f.s.	full scale
FT	Flow Transducer
g	gas (state)
GC	Glassy Carbon
GE	General Electric
GFR	Gas Fast Reactor
GIF	Generation IV International Forum
GHG	Green House Gas
GWP	Global Warming Potential
HCFC	Hydro-Chloro-Fluoro-Carbon
HFC	Hydro-Fluoro-Carbon
HHV	Higher Heating Value
HMT	Heat Mass Transfer
HP	High Pressure (turbine)
HT	Heat Transfer
HTC	Heat Transfer Coefficient
HTD	Heat Transfer Division
HTE	High-Temperature Electrolysis
HTR	High Temperature Reactor
HTTR	High Temperature engineering Test Reactor
HVAC & R	Heating Ventilating Air-Conditioning and Refrigerating
HWR	Heavy Water Reactor
HX	Heat eXchanger
IAEA	International Atomic Energy Agency (Vienna, Austria)
ICONE	International Conference On Nuclear Engineering
ID	Inside Diameter
ig	inlet gas (temperature)
INEEL	Idaho National Engineering and Environmental Laboratory (USA)
IP	Intermediate-Pressure (turbine)
IPPE	Institute of Physics and Power Engineering (Obninsk, Russia)
I/S	Iodine-Sulphur
JAEA	Japan Atomic Energy Agency
JAERI	Japan Atomic Energy Research Institute
JSME	Japan Society of Mechanical Engineers
KAERI	Korea Atomic Energy Research Institute (South Korea)
KPI	Kiev Polytechnic Institute (nowadays National Technical University of Ukraine “KPI”) (Kiev, Ukraine)
KP-SKD	Channel Reactor of Supercritical Pressure (in Russian abbreviations)
l	liquid (state)
LCA	Life-Cycle Analysis
LFR	Lead-cooled Fast Reactor
LGR	Light-water Graphite-moderated Reactor
LHV	Lower Heating Value
LMFBR	Liquid-Metal Fast-Breeder Reactor
LNG	Liquefied Natural Gas
LP	Low Pressure (turbine)
LOCA	Loss Of Coolant Accident
LOECC	Loss Of Emergency Core Cooling
Ltd.	Limited
LTE	Low-Temperature Electrolysis
LWR	Light Water Reactor
M	molarity (mol per litter (unit))
MEI	Moscow Power Institute (Moscow, Russia) (In Russian abbreviations)
MIT	Massachusetts Institute of Technology (Cambridge, MA, USA)
Mix Ch	Mixing Chamber (deaerator)
MOX	Mixed Oxide (nuclear fuel)
MSR	Molten Salt Reactor
NASA	National Aeronautics and Space Administration (USA)
NED	Nuclear Engineering Division
NIKIET	Research and Development Institute of Power Engineering (Moscow, Russia) (in Russian abbreviations)
NIST	National Institute of Standards and Technology (USA)
NPP	Nuclear Power Plant
NRC	National Regulatory Commission (USA)
OD	Outside Diameter
ODP	Ozone Depletion Potential
PBMR	Pebble-Bed Modular Reactor
PC	Personal Computer
PDT	Pressure Differential Transducer
PEM	Proton Exchange Membrane (Polymer Electrolyte Membrane)
PHEV	Plug-in Hybrid Electric Vehicle
PHWR	Pressurized Heavy-Water Reactor
Ph.D.	Philosophy Degree
PLC	Programmable Logic Controller
POCP	Photochemical Ozone Creation Potential
ppb	parts per billion
ppm	parts per million
PT	Pressure Tube (or Pressure Transducer)
PV	Pressure Vessel (reactor)
PWAC	Pratt & Whitney AirCraft
PWR	Pressurized Water Reactor
R	Refrigerant
RAD	RadioActive Radiation
RAS	Russian Academy of Sciences
RBMK	Reactor of Large Capacity Channel type (in Russian abbreviations)
RDE	Rotating Disk Electrodes
R&D	Research and Development
RDIPE	Research and Development Institute of Power Engineering (Moscow, Russia) (NIKIET in Russian abbreviations)

RMS	Root-Mean-Square (error or surface roughness)
RPV	Reactor Pressure Vessel
RSC	Russian Scientific Centre
RT	propulsion fuel (in Russian abbreviations)
RTD	Resistance Temperature Detector
s	solid (state)
SCP	SuperCritical Pressure
SCR	SuperCritical Reactor
SCW	SuperCritical Water
SCWO	SuperCritical Water Oxidation technology
SCWR	SuperCritical Water-cooled Reactor
SFL	Supercritical Fluid Leaching
SFR	Sodium Fast Reactor
S/I	Sulphur-Iodine
SKD	SuperCritical Pressure (in Russian abbreviations)
SMR	Steam-Methane-Reforming (process)
SOFC	Solid-Oxide Fuel Cell
SS	Stainless Steel
T	fuel (in Russian abbreviation)
TC	ThermoCouple
TE	TEmperature
TECO	TEmperature of CO_2
TS	Test Section
TsKTI	Central Boiler-Turbine Institute (St.-Petersburg, Russia) (in Russian abbreviations)
UCG	Uranium-Carbide Grit pored over with calcium (nuclear fuel)
UK	United Kingdom
U.K.A.E.A.	United Kingdom Atomic Energy Authority (UK)
UNESCO	United Nations Educational, Scientific and Cultural Organization (Paris, France)
UOIT	University of Ontario Institute of Technology
US or USA	United States of America
USSR	Union of Soviet Socialist Republics
VHTR	Very High-Temperature Reactor
VNIIAM	All-Union Scientific-Research Institute of AtomicMachineBuilding (Russia) (in Russian abbreviations)
VTI	All-Union Heat Engineering Institute (Moscow, Russia) (in Russian abbreviations)
VVER	Water-Water Power Reactor (in Russian abbreviations)
wt	weight
WTI	West Texas Intermediate
WWPR	Water-Water Power Reactor ("VVER" in Russian abbreviations)
XRD	X-Ray Diffraction

References

1. *Kirillov, P.L.*, *Pomet'ko, R.S.*, *Smirnov* et al., 2005. Experimental study on heat transfer to supercritical water flowing in vertical tubes, Proceedings of the International Conference GLOBAL-2005 "Nuclear Energy Systems for Future Generation and Global Sustainability", Tsukuba, Japan, October 9–13, Paper No. 518, 8 pages.

2. *Pis'mennyy, E.N.*, *Razumovskiy, V.G.*, *Maevskiy E.M.* et al., 2005. Experimental study on temperature regimes to supercritical water flowing in vertical tubes at low mass fluxes, Proceedings of the International Conference GLOBAL-2005 "Nuclear Energy Systems for Future Generation and Global Sustainability", Tsukuba, Japan, October 9–13, Paper No. 519, 9 pages.

3. *Pioro, I.L.* and *Khartabil, H.F.*, 2005. Experimental study on heat transfer to supercritical carbon dioxide flowing upward in a vertical tube, Proceedings of the 13th International Conference on Nuclear Engineering (ICONE-13), Beijing, China, May 16–20, Paper No. 50118, 9 pages.

4. *Guo, Y.*, *Bullock, D.E.*, *Pioro, I.L.* and *Martin, J.*, 2006. Measurements of sheath temperature profiles in LVRF bundles under post-dryout heat transfer conditions in Freon, Proceedings of the 14th International Conference on Nuclear Engineering (ICONE-14), July 17–20, Miami, Florida, USA, Paper #89621, 9 pages.

5. *Bezrodny, M.K.*, *Pioro, I.L.* and *Kostyuk, T.O.*, 2005. Transfer Processes in Two-Phase Thermosyphon Systems. Theory and Practice, (In Russian), 2nd edition, Augmented and Revised, Fact Publ. House, Kiev, Ukraine, 704 pages.

6. *Leung, L.K.H.*, *Pioro, I.L.* and *Bullock, D.E.*, 2003. Post-dryout surface-temperature distributions in a vertical freon-cooled 37-element bundle, Proceedigns of the 10th International Topical Meeting on Nuclear Reactor Thermal Hydraulics (NURETH-10), Seoul, Korea, October 5–9, Paper C00201, 13 pages.

7. *Pioro, I.L.*, *Groeneveld, D.C.*, *Leung, L.K.H.* et al., 2002a. Comparison of CHF measurements in horizontal and vertical tubes cooled with R-134a, International Journal of Heat and Mass Transfer, 45 (22), pp. 4435– 4450.

8. *Pioro, I.L.*, *Groeneveld, D.C.*, *Doerffer, S.S.* et al., 2002b. Effects of flow obstacles on the critical heat flux in a vertical tube cooled with upward flow of R-134a, International Journal of Heat and Mass Transfer, 45 (22), pp. 4417–4433.

9. *Pioro, I.L.*, *Groeneveld, D.*, *Cheng, S.C.* et al., 2001. Comparison of CHF measurements in R-134a cooled tubes and the water CHF look-up table, International Journal of Heat and Mass Transfer, 44 (1), pp. 73–88.

10. *Pioro, I.L.*, *Cheng, S.C.*, Vasić, A. and *Felisari, R.*, 2000. Some problems for bundle CHF prediction based on CHF measurements in simple flow geometries, Nuclear Engineering and Design, 201 (2–3), pp. 189–207.

11. *Pioro I.L.*, 1999. Experimental evaluation of constants for the Rohsenow pool boiling correlation, International Journal of Heat and Mass Transfer, 42, pp. 2003–2013.

12. *Pioro, I.L.*, 1992. Maximum heat-transferring capacity of two-phase thermosiphons with separate vapor and condensate streams, Heat Transfer Research, 24 (4), pp. 535–542.

13. *Pioro, L.S.* and *Pioro, I.L.*, 1997. Industrial Two-Phase Thermosyphons, Begell House, New York, NY, USA, 288 pages.

14. *Kichigin, A.M.* and *Pioro, I.L.*, 1992. Analysis of methods for detecting dryout and burnout fluxes, Heat Transfer Research, 24 (7), pp. 957–964.

15. *Pioro, I.L.* and *Kalashnikov, A.Yu.*, 1988. Maximum heat transfer in two-phase thermosyphons with external down-flow channel, Applied Thermal Sciences, 1 (2), pp. 62–67.

16. *Pioro, I.L.*, 1982. Investigation of closed two-phase thermosyphons used for cooling of melting converters, (In Russian), Applied Problems of Heat Transfer and Hydrodynamics, Naukova Dumka, Publishing House, Kiev, Ukraine, pp. 76–79.

17. *Coleman, H.W.* and *Steele, W.G.*, 1999. Experimentation and Uncertainty Analysis for Engineers, 2nd edition, J. Wiley & Sons, Inc., New York, USA, 275 pages.

18. *Hardy, J.E.*, *Hylton, J.O.*, *McKnight, T.E.* et al., 1999. Flow Measurement Methods and Applications. J. Wiley & Sons, Inc., New York, NY, USA, pp. 207–208.

19. *Guide* to the Expression of Uncertainty in Measurement, 1995. Corrected and Reprinted, International Bureau of Weights and Measures and other International Organizations, 101 pages.

20. *Holman, J.P.*, 1994. Experimental Methods for Engineers, 6th edition, McGraw-Hill, Inc., New York, NY, USA, 616 pages.

21. *Moffat, R.J.*, 1988. Describing the uncertainties in experimental results, Experimental Thermal and Fluid Science, 1, pp. 3–17.

22. *Gortyshov, Yu.F.*, *Dresvyannikov, F.N.*, Idiatullin, N.S. et al., 1985. Theory and Technique of Thermophysical Experiment, Textbook for Technical Universities, (In Russian), Editor V.K. Shchukin, Energoatomizdat Publishing House, Moscow, Russia, 360 pages.

23. *Topping, J.* 1971. Errors of Observation and Their Treatment, 3rd edition, Chapman and Hall Ltd., London, UK, 119 pages.

24. *Mark's* Standard Handbook for Mechanical Engineers, 1996. Editors: Eu.A. Avallone and Th. Baumeister III, McGraw-Hill, New York, NY, USA, p. 16-2.

25. *National* Institute of Standards and Technology, 2010. NIST Reference Fluid Thermodynamic and Transport Properties-REFPROP. NIST Standard Reference Database 23, Ver. 9.0. Boulder, CO, U.S.: Department of Commerce.

26. *The Temperature* Handbook, 2000. OMEGA Engineering, Inc., 21st Century Edition, Vol. MM.

27. *White, F.M.*, 1994. Fluid Mechanics. Third edition, McGraw-Hill, Inc., New York, NY, USA, pp. 364–365.

28. *The Flow* and Level Handbook, 2000. OMEGA Engineering, Inc., 21st Century Edition, Vol. MM, (Transactions, Vol. 4, p. 22).

29. *Pioro, I., Zvorykina A.*, 2012. Some important aspects for experimental papers: Part 1. Typical heat-transfer / thermalhydraulics test facility and practical recommendations for performing experiments, Technological Systems (Ukraine), Vol. 1 (58). P. 17–28. ISSN 2074-0603.